JOURNAL OF MATERIALS SCIENCE 16 (1981) 994–1000

Crystallization of sputter deposited amorphous MoNi

J. L. BRIMHALL, H. E. KISSINGER, R. WANG
Pacific Northwest Laboratory Richland, Washington 99352, USA

A crystallization temperature of ~ 1000 K was observed for an amorphous alloy of MoNi. Recovery of the amorphous matrix prior to crystallization was noted, however. During crystallization, a Mo-rich phase and a Ni-rich phase first precipitated, then reacted to form the equilibrium δ-phase. Exaggerated grain growth or secondary crystallization of the δ-phase occurred upon extensive annealing. This multi-step mechanism contrasts with that in the amorphous μ-phase. The multi-step crystallization process is similar to, though not as complex as, that observed in many liquid-quenched alloys. In particular, no incipient stage of crystallization was noted.

1. Introduction

To determine the thermal stability of amorphous MoNi and to gain additional knowledge of the crystallization mechanisms, the annealing behaviour was studied using transmission electron microscopy (TEM), X-ray analysis and electrical resistivity measurements. An alloy of 50% Mo–50% Ni forms an intermetallic δ-phase in the crystalline state. Because the crystal structure of this phase is related to that of the FeW and MoCo μ-phase, a comparison of the crystallization behaviour in the different systems was made. Amorphous alloys of FeW and MoCo with the μ-phase composition have crystallization temperatures > 1000 K [1–3]. It was expected that the amorphous MoNi alloy would also exhibit this high thermal stability. In addition, the similarities and/or differences in the annealing behaviour between this alloy and liquid-quenched amorphous alloys were noted.

2. Experimental procedure

The alloys were prepared by high-rate sputter deposition. The target material was a pressed powder compact of molybdenum and nickel. Sputtering was performed in krypton at a rate of 25 μm h. The substrate was cooled by liquid nitrogen. The thickness of the final deposit was approximately 200 μm and the composition of the deposit was 50 at %Mo + 50 at %Ni as determined by electron probe microanalysis.

Specimens suitable for TEM were cut from the deposit and annealed for various times and at various temperatures in a vacuum of 3×10^{-4} Pa. Specimens were thinned for TEM examination after the annealing treatments. X-ray Debye–Scherrer photographs were taken on the same specimens used for TEM work.

The electrical resistivity was measured with a Rosemont commutating bridge using a four-probe technique. Slices measuring approximately 1 mm by 10 mm were cut from the original deposit. In order to protect the very fragile specimens from damage during handling, they were mounted in a special probe tip which formed a rigid, cage-like structure. All annealing and measurements were then made without removing the specimen from the mounting. The resistance measurements were made at 296 K and 78 K following one-hour, high-temperature anneals. The absolute values of the resistivities were difficult to determine and all values were normalized by dividing by the value for the original amorphous phase.

3. Experimental results

The electrical resistivity, ρ, and temperature coefficient of resistivity ρ_T/ρ_{78}, were well correlated with the microstructural changes observed during recovery and crystallization. A decrease in ρ and and increase in ρ_T/ρ_{78} coincided with the formation of Mo-rich and Ni-rich metallic phases. A subseqeunt increase in ρ and decrease in ρ_T/ρ_{78}

0022–2461/81/040994–07$02.70/0

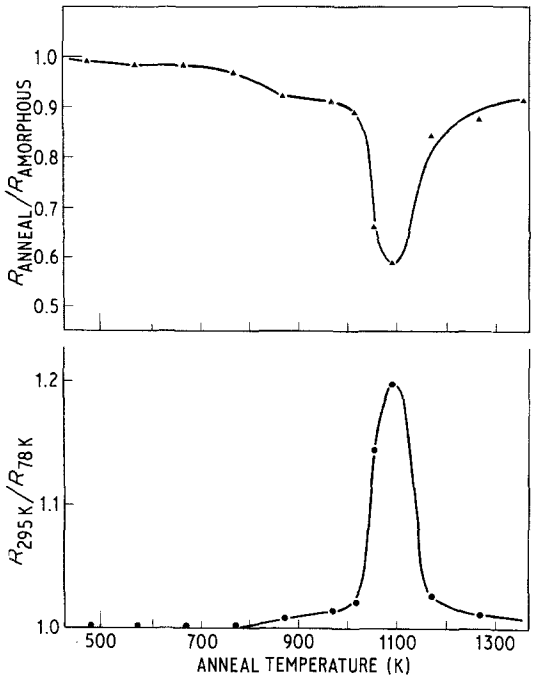

Figure 1 (a) Electrical resistance of amorphous MoNi measured at 78 K as a function of annealing temperature. Resistance is normalized to the starting value. (b) Ratio of resistance at 78 K to resistance at 295 K as a function of annealing temperature.

coincided with the reaction of the intermediate phases to form equilibrium δ-phase. There was also evidence for secondary recrystallization or exaggerated grain growth at higher temperatures.

3.1. Electrical resistivity

The electrical resistivity as a function of annealing temperature passed through a minimum value at ~1070 K. This minimum in the resistivity coincided with a maximum in the temperature coefficient of resistivity. The change in resistivity as a function of annealing was characterized by a small drop between 770 and 870 K, a sharp drop between 970 and 1070 K, and an increase beyond the 1070 K anneal (Fig. 1). Recovery or relaxation was indicated by the small drop, and the sharp drop indicated the onset of crystallization. This sharp drop can be attributed to formation of crystalline metallic phases which have an inherent low resistivity. The increase in resistivity at temperatures greater than 1070 K coincided with the emergence of the δ-phase. The δ-phase is an intermetallic compound with a high resistivity. The resistivity of the crystalline δ-phase was observed to be almost as great as that of the amorphous phase.

A measure of the temperature coefficient of resistance is given by the ratio R_{295}/R_{78}. This varied with the phases present (Fig. 1b). For the amorphous condition, the ratio was essentially unity. A weak or non-existent temperature coefficient of resistivity has been reported for amorphous metals [4]. This resistivity ratio tended to reach a peak value at an annealing temperature at which the greatest amount of metallic phase was present. Crystalline metals have a strong temperature dependence of resistivity. The δ-phase was observed to have a low temperature coefficient as the ratio again decreased to unity when the δ-phase formed.

3.2. Microstructure

Subtle microstructural changes (recovery) were observed prior to massive crystallization of the matrix. The crystallization occurred in two stages: the formation of a Mo-rich and Ni-rich crystal phase was followed by transformation to the δ-phase. There was evidence of a secondary recrystallization of the δ-phase with prolonged annealing.

3.3. As-deposited and recovered structure

A slight coarsening of the featureless amorphous phase was observed after annealing below the crystallization temperature. Crystals of MoO_2 formed during these low-temperature anneals. The microstructure in the as-deposited condition was essentially featureless (Fig. 2). The selected-area diffraction (SAD) pattern shows one bright, diffuse ring plus several larger, but fainter diffuse rings. This structure is identical to that reported for FeW, MoCo [3] and NbNi [5] and is characteristic of most amorphous alloys. A portion of the bright ring in Fig. 2 was used to form a dark-field (DF) image, which also revealed an essentially featureless structure. Some extremely small "bright" spots could be revolved in DF in the thinner regions of the foil. It is believed, however, that these "bright" spots are not indicative of a true microcrystalline structure [6].

There was no crystallization of the main constituents after such treatments as 24 h at 870 K or 6 h at 1020 K, but recovery was evident. The diffuse diffraction rings appeared to be somewhat sharper after these annealing treatments than in the as-deposited state. No extra rings were noted, however. Very small white spots could clearly be resolved under the proper diffracting conditions (Fig. 3b). These correlated with the black spots

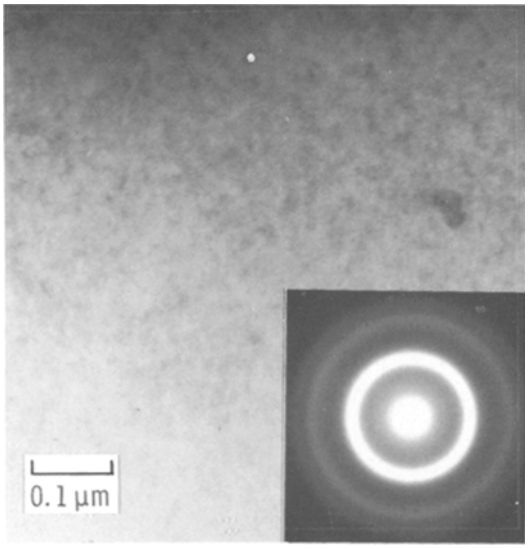

Figure 2 Microstructure of as-deposited MoNi alloy showing featureless amorphous structure.

seen in bright field (BF) (Fig. 3a). The size of these spots definitely increased with annealing temperature, but there was little size change with time, e.g., between 1 h and 6 h at 1020 K.

MoO_2 crystals formed within the still amorphous matrix in the temperature range above 850 K (Fig. 4). The volume fraction of oxide particles shown in the figure is ~ 0.5%. The volume fraction saturated after several hours of annealing, evidently as a result of oxygen depletion of the matrix. The oxide particles account for ~ 0.4 at % oxygen.

3.4. Crystallized structures

The microstructural and phase development during crystallization was complex and temperature dependent. Results are presented separately for three annealing temperatures: 970, 1070 and 1170 K. The most extensive isothermal results were obtained for 1070 K. The results will show an initial transformation to the metastable phases $Mo + MoNi_3$ at the lower temperatures and Mo + Ni solid solution at the higher temperatures. All these phases eventually transformed to the equilibrium δ-MoNi with prolonged annealing. Both types of metastable phases were observed to co-exist at intermediate temperatures.

3.4.1. 970 K

The amorphous structure crystallized into a two-phase, lamellar structure during prolonged annealing at 970 K (Fig. 5). The two phases are identified as molybdenum and $MoNi_3$ ($Mo + MoNi_3$). X-ray microanalysis using a scanning TEM revealed the dark bands to be molybdenum and the light bands to be $MoNi_3$. Approximately 30–50% of the structure was crystallized after this annealing treatment. The remaining amorphous phase was a recovered structure similar to that shown in Fig. 3.

Diffraction analysis showed all the molybdenum bands to have a similar orientation and all the $MoNi_3$ bands to have a similar orientation. In many cases certain crystallographic directions were aligned in the Mo and $MoNi_3$ indicating a morphological

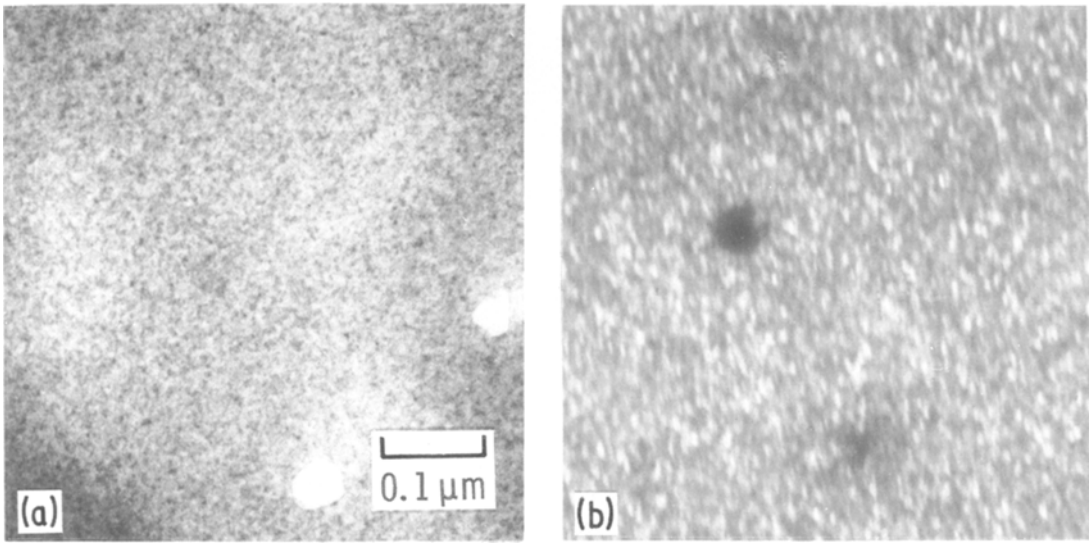

Figure 3 Microstructure of amorphous MoNi annealed for 1 h at 1020 K: (a) BF showing small black spots or grainy structure, (b) DF showing bright diffracting regions.

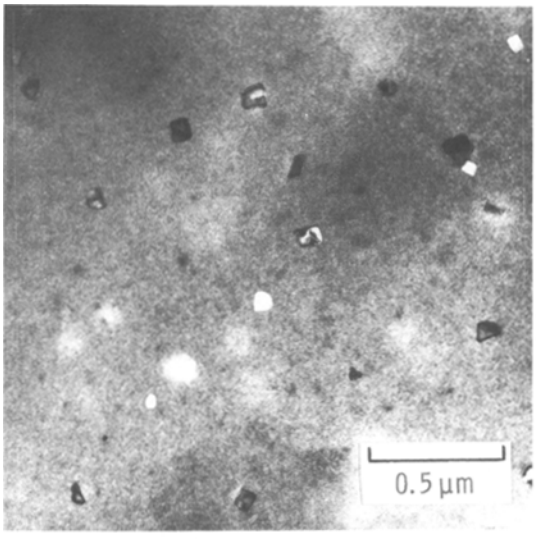

Figure 4 Microstructure of amorphous MoNi annealed for 6 h at 970 K showing isolated crystals of MoO_2.

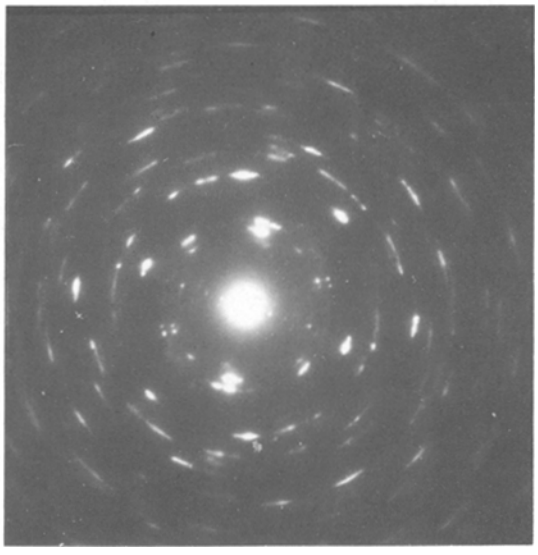

Figure 6 SAD pattern from large area of lamellar structure. Some δ-phase is evident from the SAD pattern.

relationship of the two phases. The Mo(1 1 0) is parallel to $MoNi_3$(0 1 0) and the Mo(0 0 1) is parallel to $MoNi_3$(1 0 0).

The presence of the emerging δ-phase was detected by forming a SAD pattern from a very large area. The spots representing large d spacings in Fig. 6 arise from the δ-phase. This phase appeared as isolated patches of small grains within the Mo + $MoNi_3$ structure. The polycrystalline nature of the diffraction pattern in Fig. 6 is a result of including many differently oriented lamellar regions within the SAD pattern.

3.4.2. 1070 K

Both the lamellar-type structure mentioned above and a fine, equiaxed crystal structure formed at the higher temperature of 1070 K. After 0.5 h at 1070 K, small, widely scattered regions of the lamellar Mo + $MoNi_3$ were detected (Fig. 7). The surrounding matrix, however, showed evidence of crystallite formation, as indicated by the isolated

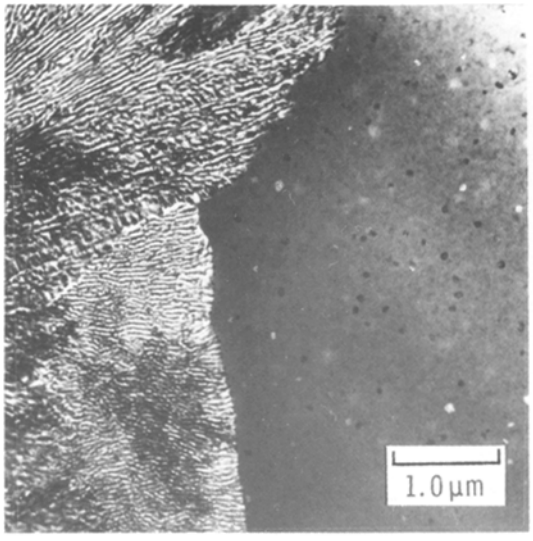

Figure 5 Microstructure of amorphous MoNi annealed for 48 h at 970 K showing (Mo + $MoNi_3$) crystalline region growing into amorphous region.

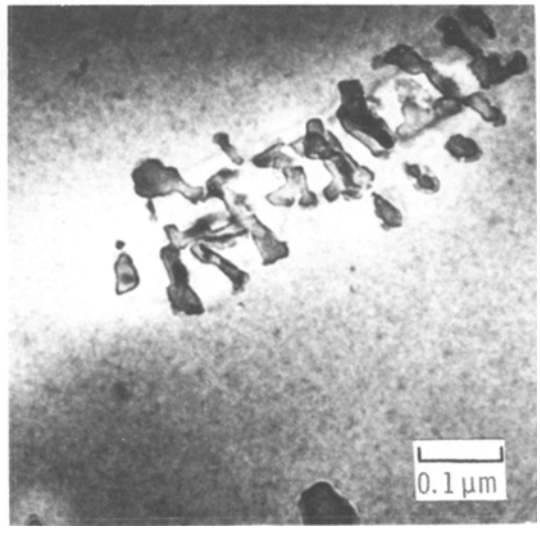

Figure 7 Microstructure of MoNi annealed for 0.5 h at 1070 K showing isolated patch of (Mo + $MoNi_3$) structure.

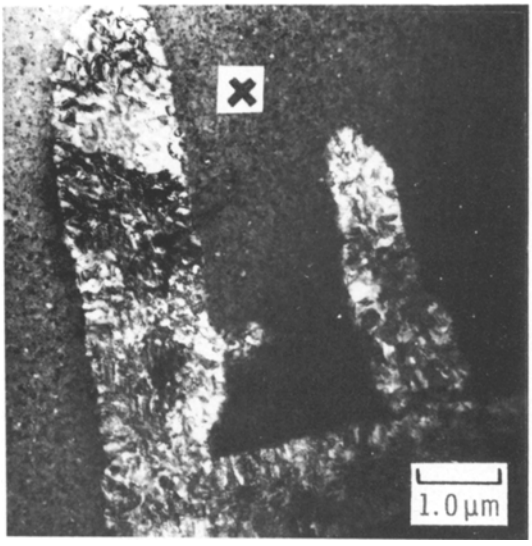

Figure 8 Microstructure of MoNi annealed for 2 h at 1070 K indicating extensive crystallite formation.

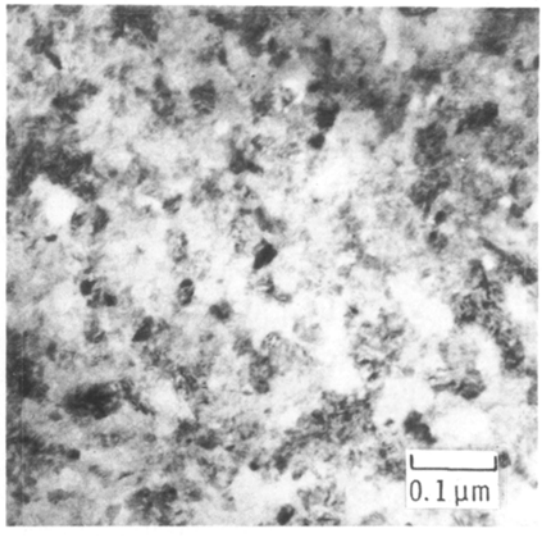

Figure 9 Microstructure of MoNi annealed for 2 h at 1070 K; high magnification of fine crystallite region marked X in Fig. 8.

black spots in Fig. 7. Dark-field microscopy revealed these to be diffracting particles, but distinct from the MoO_2 crystals which were much larger.

Extensive regions of both the lamellar Mo + $MoNi_3$ and the fine-grain structure were observed after 2 h at 1070 K (Fig. 8). The lamellar morphology of the Mo + $MoNi_3$ was not as pronounced as at 970 K, but analysis again revealed alternating regions of Mo and $MoNi_3$. The fine-grain region appeared to contain much unidentifiable substructure (Fig. 9). SAD patterns and X-ray diffraction indicated a mixture of Mo, α-Ni (Ni + Mo in solid solution) and a trace of δ-MoNi for the fine-grain region. Lattice parameter measurements of the α-Ni phase indicated about 20–25 at %Mo in solution. Due to the fine grain size and complex structure, it was not possible to assign a specific phase to a specific grain. Some SAD patterns indicated *d* spacings that were close to the δ-phase, but the crystal structure was not quite right. This could represent a disordered or non-equilibrium δ-phase that is a precursor to the equilibrium δ-phase.

Grain growth of the fine-grain structure as well as growth of the lamellar structure continued with increased annealing time. The distribution of the lamellar structure Mo + $MoNi_3$ was very inhomogeneous on a TEM scale and the fractional amount was difficult to estimate; however, there appeared to be more of the Mo + $MoNi_3$ present after 8 h than after 2 h at 1070 K. Larger grains within the fine-grain structure could be identified as the growing δ-phase. Very large δ-phase grains were present after prolonged annealing (48 h at 1070 K), which were indicative of a secondary recrystallization process (Fig. 10). Very little Mo, $MoNi_3$ or α-Ni was present after the prolonged anneal. The very fine grain size and the apparent high defect structure of the grains would provide a high driving force for the secondary recrystallization process.

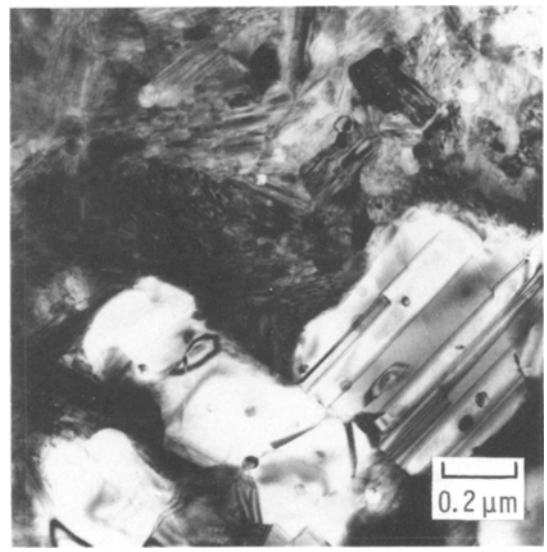

Figure 10 Microstructure of MoNi annealed for 48 h at 1070 K. Mostly all δ-phase.

3.4.3. 1170 K

X-ray and electron diffraction indicated predominantly δ-phase with some molybdenum and α-Ni solid solution after annealing for 0.5 h at 1170 K. No $MoNi_3$ was present. The structure was complex with a high degree of faulting within the grains. The microstructure was very similar to that shown in Fig. 10, in which some of the δ-grains were considerably larger than the average. This would indicate that a secondary recrystallization process had already begun after this short time at 1170 K.

4. Discussion

Sputter-deposited amorphous MoNi alloy was observed to have a thermal stability comparable to μ-phase MoCo which is closest to it in elemental form, but the crystallization mechanism was found to be different in the two systems. The changes in electrical resistivity suggested a multi-step process rather than a direct transformation to the equilibrium phase as occurs in MoCo. The TEM examination correlated well with the resistivity observations and showed the precipitation of Mo-rich and Ni-rich phases which subsequently reacted to form the equilibrium δ-phase. Extensive annealing for longer times or at higher temperatures produced a secondary recrystallization of the δ-phase which resulted in large δ-grains.

The type of nickel-rich phase and overall mode of crystallization in amorphous MoNi was strongly dependent on the annealing temperature. Herold and Köster [7] have proposed three possible modes of crystallization for amorphous alloys: (a) polymorphous, (b) primary and (c) eutectic. At low temperatures (970 K), the reaction appeared to be a classic eutectic (or eutectoid) reaction, i.e., simultaneous crystallization of Mo and $MoNi_3$. At the reaction front, the two components separate into their respective phases. This type of reaction has been observed in a number of amorphous alloys, particularly of the metal–metalloid type [8–11]. At higher temperatures (1170 K), Mo and α-Ni nucleated randomly with a high nucleation rate. The absence of $MoNi_3$ at high temperatures is compatible with the phase diagram which shows $MoNi_3$ not to be stable above ~ 1180 K. This reaction could be classed as a primary-type crystallization in which one phase precipitates resulting in an enrichment of the remaining elements in the amorphous phase. The remaining amorphous material then transforms at a later time or higher temperature. However, the crystallization in MoNi was so rapid that it was not possible to determine precisely whether the crystallites formed simultaneously or sequentially.

At intermediate temperatures (1070 K), the inherent sluggishness of the eutectic reaction allowed time for the transformation of the remaining amorphous matrix by way of the primary-type reaction described above. Hence a multi-phase structure Mo + $MoNi_3$ and Mo + α-Ni developed. Both phase regions then slowly transform to the δ-phase. This behaviour was somewhat different from the amorphous μ-phase alloys that appeared to go directly from the amorphous state to the final equilibrium phase. There is no obvious reason for this difference in crystallization behaviour. It is apparently an easier energy path to follow for the MoNi to first precipitate as simple crystalline phases and to subsequently transform to the complex δ-phase. The enthalpy of formation at 973 K of δ-MoNi ($-1000\,J\,mol^{-1}$) is less negative than that of μ-MoCo ($-4000\,J\,mol^{-1}$), and this difference becomes greater with increase in temperature [12]. It may be the small differences in thermodynamic properties that dictate the particular crystallization reaction sequence.

The formation of a metastable phase in the MoNi prior to the final equilibrium phase showed some similarity in behaviour to liquid-quenched eutectic alloys, but there were differences. Masumoto and Maddin [13] proposed a multi-stage process for crystallizaton in amorphous alloys of eutectic composition: (a) incipient crystallization, (b) metastable stage MS-I, (c) metastable stage MS-II, and (d) stable phase. All amorphous alloys do not necessarily follow these steps exactly and there are variations in the sequence. In MoNi, however, there was no incipient crystallization and only one metastable stage occurred. Furthermore, the metastable phases in MoNi can be found in the phase diagram unlike some of the metastable phases in the eutectic alloys. In quenched amorphous NbNi, for example, a metastable M-phase formed prior to the equilibrium phase although the M-phase is not found in the NbNi phase diagram [5].

The crystallization process in MoNi is therefore simpler than in many of the eutectic alloys, although it is not as simple or straightforward as anticipated. An explanation for the crystallization mechanism in these amorphous alloys of compound composition probably lies in the details of

the particular phase diagram and subtle differences in thermodynamic properties.

Structural rearrangements or recovery which occurred just prior to crystallization were similar in MoNi and the μ-phase alloys. The slight drop in resistivity indicated a recovery process that also coincided with the appearances of the small clusters seen by dark-field microscopy. Relaxation or recovery of the amorphous structure has been observed in a number of amorphous alloys [14–16] and in this respect, MoNi is similar in behaviour to eutectic-type amorphous alloys. There was no firm evidence, however, that the small domains or clusters are the nuclei of the subsequent crystallization.

The presence of MoO_2 crystals in the amorphous structure is evidence that a significant amount of oxygen was entrapped during the sputter deposition process. Since MoO_2 was also found in amorphous MoCo alloys, it is believed that the oxygen came from the molybdenum powders. Similar internal oxidation has recently been seen in other amorphous alloys. In liquid-quenched ZrCu and NbNi alloys containing $\geqslant 2$ at % oxygen, a ternary oxide phase formed prior to the formation of the crystalline metallic phases [17]. The diffusion of oxygen in these amorphous alloys must be significantly greater than the major elements as the oxide forms in a temperature regime considerably below the normal crystallization temperature.

5. Conclusions

(a) Amorphous MoNi shows a high thermal stability ($\geqslant 1000$ K), comparable to the amorphous μ-phase alloys.

(b) The resistivity changes during annealing correlated very well with microstructural changes.

(c) Crystallization occurred in a two-step process; an initial precipitation of a Mo-rich and Ni-rich phase which then reacted to form the equilibrium δ-phase. Secondary recrystallization of the δ-phase occurred upon extensive annealing.

(d) The crystallization behaviour is more complex than that in armouphous μ-phase alloys, but no obvious explanations are apparent.

Acknowledgement

This work was supported by the Basic Science Division of the Department of Energy, and prepared for the US Department of Energy under contract DE-AC06-76RLO 1830.

References

1. R. WANG, M. D. MERZ, J. L. BRIMHALL and S. D. DAHLGREN, "Rapidly Quenched Metals III", edited by B. Canton (Metals Society, England, 1979) p. 420.
2. R. WANG, M. D. MERZ and J. L. BRIMHALL, *Scripta Met.* **12** (1978) 1037.
3. J. L. BRIMHALL, H. E. KISSINGER and R. WANG, *J. Mater. Sci.* **15** (1980) 2605.
4. H. J. GÜNTHERODT and H. U. KÜNZI, "Metallic Glasses", (ASM, Metals Park, Ohio 1978) p. 248.
5. R. C. RUHL, B. C. GIESSEN, M. COHEN and N. J. GRANT, *Acta Metallogr.* **15** (1967) 1693.
6. P. CHOUDHARI, J. F. GRACZYK and S. R. HERD, *Phys. Stat. Solidi (b)* **51**(1972) 81.
7. U. HEROLD and U. KÖSTER, "Rapid Quenched Metals III", edited by B. Cantor (Metals Society, England, 1979) p. 281.
8. J. L. WALTER, S. F. BARTRAM and P. R. RUSSELL, *Met. Trans.* **9A** (1978) 803.
9. U. KÖSTER and U. HEROLD, *Scripta Met.* **12** (1978) 75.
10. P. G. BOSWELL, *ibid* **11** (1977) 701.
11. M. KACZOROWSKI, J. KOZUBOWSKI, B. DRABOWSKI and H. MATYJA, *J. Mater. Sci.* **13** (1978) 407.
12. P. J. SPENCER and F. H. PUTLAND, *J. Chem. Thermodynamics* 7 (1975) 531.
13. T. MASUMOTO and R. MADDIN, *Mater. Sci. Eng.* **19** (1975) 1.
14. A. J. KERNS, D. E. POLK, R. RAY and B. C. GIESSEN, *ibid* **38** (1979) 49.
15. H. S. CHEN and E. COLEMAN, *Appl. Phys. Lett.* **28** (1976) 245.
16. T. EGAMI, *Mater. Res. Bull.* **13** (1978) 557.
17. C. E. DUBE and B. C. GEISSEN, "Rapidly Quenched Metals III", (Metals Society, England, 1979) p. 220.

Received 16 July and accepted 4 September 1980.